Strain and oxygen vacancy ordering in SrTiO_{3}: Diffuse x-ray scattering studies

Yongsam Kim, Ankit S. Disa, Timur E. Babakol, Xinyue Fang, and Joel D. Brock

Phys. Rev. B **92**, 064105 — Published 7 August 2015

DOI: 10.1103/PhysRevB.92.064105

Strain and Oxygen Vacancy Ordering in $SrTiO_3$: Diffuse X-ray Scattering Studies

Yongsam Kim,[1,2,*] Ankit S. Disa,[1,3] Timur E. Babakol,[1] Xinyue Fang,[1,4] and Joel D. Brock[1,†]

[1] *School of Applied & Engineering Physics, Cornell University, Ithaca, NY 14853, USA*
[2] *Pohang Accelerator Laboratory, Pohang University of Science and Technology, Pohang 790-834, Republic of Korea*
[3] *Department of Applied Physics, Yale University, New Haven, Connecticut 06520, USA*
[4] *Department of Physics, University of Illinois at Urbana-Champaign, Urbana, IL 61801, USA*

We report systematic diffuse x-ray scattering measurements of the elastic strain fields generated by oxygen vacancies in strained bulk $SrTiO_3$ crystals. Diffuse x-ray scattering has been used for decades to measure the elastic strain fields generated by point defects based on the assumptions that the defects are randomly distributed and uncorrelated. We find for $SrTiO_3$ that (i) there are correlations between oxygen vacancies with different orientations, (ii) we can manipulate the relative concentrations of the three orientations via applied stress, and (iii) the oxygen vacancies cluster around the edge dislocations, creating a two-dimensional distribution.

I. INTRODUCTION

Complex oxides exhibit a vast range of functional properties such as high dielectric permittivity, piezoelectricity, ferroelectricity, superconductivity, ferromagnetism, colossal magnetoresistance, and multiferroic behavior. Moreover, heterostructures of ultrathin (single unit cell thick) layers of the oxides with the perovskite structure can be fabricated with atomically sharp interfaces and with a degree of crystalline perfection rivaling that previously attained only in semiconducting systems[1]. The range of phenomena exhibited by interfaces and heterostructures of these oxide materials is very rich. As an example, the $SrTiO_3/LaAlO_3$ interface can host a 2D electron gas and exhibit superconducting, insulating, or metallic conduction[2]. The electrical properties of the $SrTiO_3/LaAlO_3$ interface are believed to be determined by the relative contributions of three factors: oxygen vacancies, structural deformations (including cation disorder), and electronic interface reconstructions[3]. The structural imperfections, such as defects or lattice mismatch at the interface, generate strain, which can be used to engineer and enhance the properties of the oxide[4]. Oxygen vacancies are of particular importance, as they can change the properties of $SrTiO_3$ from that of a wide bandgap insulator to that of a conductor[5,6].

Freedman and coworkers[7,8] calculated the elastic response of a $SrTiO_3$ crystal to various vacancies . They found that the (reconstruction averaged) elastic dipole tensor is anisotropic but nearly traceless for an oxygen vacancy. Thus, adding the displacement fields of the three different vacancy orientations together produces a negligible net displacement field. To experimentally confirm this interesting prediction, we performed diffuse x-ray scattering studies of oxygen deficient $SrTiO_3$ to measure the net displacement field directly. In a previous study[9], we demonstrated that

1. the net lattice distortion field from a uniform collection of oxygen vacancies is below our experimental detection limit;

2. the relative concentrations of the three possible orientations of oxygen vacancies can be controlled via applied stress; and,

3. the symmetry of the diffuse scattering is consistent with Freedman's result for the elastic dipole tensor.

However, the way in which the oxygen vacancies were correlated was not understood. In particular, the observed q^{-3} dependence of the diffuse scattering and how vacancy triplets could form at such low vacancy concentrations could not be explained. Here, we answer the question of the nature of the correlations between the vacancies, characterize the structure of the defect clusters, and present a self-consistent picture of oxygen vacancies in $SrTiO_3$ in which the oxygen vacancies cluster around the cores of the oriented edge dislocations introduced in the initial growth of the crystal.

II. EXPERIMENTAL DETAILS

As received, Verneuil-grown $SrTiO_3$ (001) crystals ($10\times10\times1$ mm^3) were annealed at 600 °C for 12 hours in flowing O_2 to minimize the concentration of the pre-existing oxygen vacancies (V_O). Then, in order to controllably produce oxygen vacancies, the samples were annealed in vacuum at 5×10^{-7} Torr (base pressure of 1×10^{-7} Torr) for 12 hours at 600 °C. The sample color changed from transparent to dark gray, which is a feature of oxygen deficient $SrTiO_3$ crystals. The sheet resistance of samples with Pt electrodes deposited on the surface and annealed as above was measured using the Van der Pauw method[10,11]. Since oxygen vacancies act as n-type dopants, the conductivity is a direct measure of the total vacancy density. The resulting vacancy concentration for these oxygen deficient samples is on the order of 10^{16} cm^{-3} [6,12]. During the annealing process, some samples were subjected to a uniaxial compressive stress to change the oxygen vacancy distribution. The applied uniaxial compressive stress in the surface normal (z) direction of the sample was about 3 GPa, corresponding to approximately 0.1 % strain in the z direction. This stress during annealing is expected to cause about 40 % excess

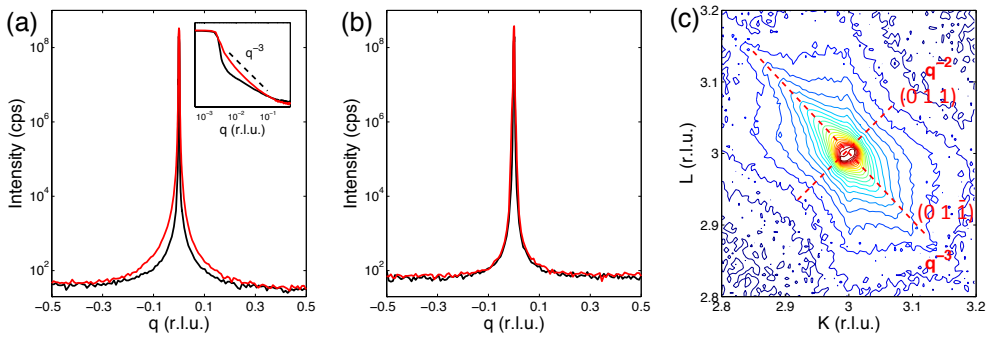

FIG. 1. (Color online) The (0 3 3) x-ray scattering profiles in the direction of (a)(0 1 $\bar{1}$) and (b)(0 1 1) of the sample annealed in vacuum under stress (red) and without stress (black) (inset : log-log scale plot with q^{-3} line). (c)The (0 3 3) reciprocal space map of the strained sample. The diffuse profiles of the strained sample in (0 1 $\bar{1}$) and (0 1 1) directions show the q^{-3} and q^{-2} dependence, respectively (the contour intensity becomes higher from blue to red color).

$(V_O)_z$ in the crystal. All samples annealed in vacuum, with and without stress, have the same color (dark gray) and sheet resistance implying that the total number of vacancies is the same. After each annealing process, the x-ray diffuse scattering was measured.

The x-ray measurements were carried out at the A2 beamline at the Cornell High Energy Synchrotron Source (CHESS). To access as much reciprocal space as possible while avoiding the Sr K-shell fluorescence, an x-ray energy of 15.54 keV was used. At room temperature, $SrTiO_3$ has the cubic perovskite structure with a lattice constant $a = 3.905$ Å. The measured resolutions (HWHM) near the (0 3 3) Bragg peak are 1.3×10^{-3}, 4.4×10^{-3}, and 2.0×10^{-3} in reciprocal lattice units (r.l.u.) in the h, k, and ℓ directions, respectively.

III. RESULTS

We first measured the (0 3 3) x-ray scattering profiles of the unstressed vacuum annealed sample. It showed no measurable increase in diffuse scattering due to the oxygen vacancies; the scattering was indistinguishable from that of an annealed sample without vacancies. Since no external stress was applied during the annealing process, this result can be understood from the fact that the oxygen vacancies occupy the three sub-lattices equally and the resulting strain fields cancel[9]. Hence, no diffuse scattering is observed from an isotropic concentration of oxygen vacancies in $SrTiO_3$.

In addition, the lattice constants of the samples with and without oxygen vacancies (unstressed) are the same within experimental error at the (0 0 5) Bragg reflection. That is, there is no measurable volume change due to the oxygen vacancies in the $SrTiO_3$ crystal, agreeing with previous reports[13,14]. Both of these experimental results are incompatible with the conventionally used diffuse scattering analysis[15–18], which is based on the assumption that the point defects are randomly distributed.

We now turn to the results of the sample annealed under stress with an excess of z-type vacancies, which shows drastically different behavior than the unstressed sample. We note again that the total oxygen vacancy concentration is the same in both samples annealed in vacuum with and without an external stress. Figure 1(a-b) shows the x-ray scattering profiles along (0 1 $\bar{1}$) and (0 1 1) directions through the (0 3 3) Bragg reflection. After annealing in vacuum with stress, the sample shows enhanced diffuse scattering along the (0 1 $\bar{1}$) (Fig. 1(a)) (red line) compared to the sample annealed in vacuum without stress (black line). This enhancement is consistent with the expected diffuse scattering from the uncompensated $(V_O)_z$ in the crystal[9]. However, the two profiles along the (0 1 1) in Fig. 1(b) are almost identical. There is no enhancement in the diffuse scattering of the strained sample along the (0 1 1) direction, even though there is an uncompensated strain field. This reveals that the symmetry of the diffuse scattering differs from the conventional case, which has strong scattering in the (0 1 1) direction and a nodal plane in (0 1 $\bar{1}$) direction at the (0 3 3) Bragg peak of a cubic crystal.

In order to investigate the diffuse scattering symmetry of the strained sample in detail, the reciprocal space map (RSM) at the (0 3 3) peak was measured (Fig. 1(c)). The (0 3 3) Bragg peak is at the center of the map, and the broad elliptical shaped diffuse scattering is the thermal diffuse scattering (TDS). The TDS lies along the (0 1 $\bar{1}$) direction and the relatively narrow diffuse scattering from uncompensated $(V_O)_z$ can be seen in addition to TDS lying along the (0 1 $\bar{1}$) direction. The RSM illustrates the unique diffuse scattering symmetry of oxygen vacancies in $SrTiO_3$. In addition to the unique symmetry, we observe that the enhanced scattering along the (0 1 $\bar{1}$) direction decreases as q^{-3}. (see inset of Fig. 1(a). This q-dependence cannot be understood as the scattering from isotropic, three-dimensional vacancies, which would have a q^{-2} dependence. As will be discussed in the next section, both of these observations can be under-

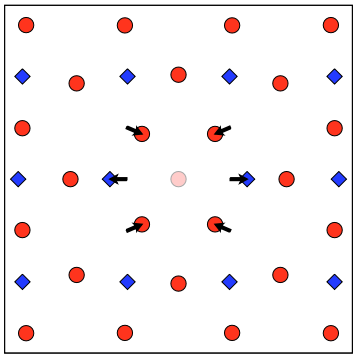

FIG. 2. (Color online) Calculated displacements around an oxygen vacancy in the Ti-O plane of $SrTiO_3$. Ti atoms expand away from the vacancy (red circle : O atoms, blue diamond : Ti atoms) from the Ref. [8]

stood in the context of scattering from oxygen vacancies clustered around oriented dislocation lines in $SrTiO_3$. In Secs. IV.A and B we discuss the diffuse scattering from oxygen vacancies in $SrTiO_3$ in general, and in Sec. IV.C we provide a clustering model to explain the anomalous q^{-3} dependence.

IV. DISCUSSION

A. Elastic dipole tensor for an oxygen vacancy in $SrTiO_3$

Freedman *et al* calculated the effective (reconstruction averaged) elastic dipole (P) and defect strain (Λ) tensors for significant point defects, including oxygen vacancies, in $SrTiO_3$ crystals[7,8]. There are three types of oxygen vacancies ($(V_O)_n$; $n = x, y, z$), distinguished by which face of the cube is missing the oxygen atom. The Sr atoms contract towards the vacancy in the Sr-O plane and Ti atoms expand away from the vacancy in the Ti-V_O-Ti direction when an oxygen atom is removed from the crystal (Fig. 2).

The associated reconstruction averaged elastic dipole tensor P for an x-type oxygen vacancy[8] is

$$P = \begin{pmatrix} 4.53 & 0.00 & 0.00 \\ 0.00 & -2.13 & 0.00 \\ 0.00 & 0.00 & -2.13 \end{pmatrix} eV. \quad (1)$$

The y and z-type tensors can be obtained by permuting the diagonal elements. The defect strain tensor follows directly from P and the elastic stiffness tensor. The resultant defect strain tensor is also nearly traceless. Thus, the lattice distortion fields of three oxygen vacancies of differing orientations located adjacent to each other almost completely cancel, producing a negligibly small net lattice distortion field.

The free energy density of the crystal as a function of the strain ε_{ij} and the number density of defects n_d is[8]

$$f(\varepsilon_{ij}, n_d) = f_0 + n_d E_d + \frac{1}{2}\mathrm{C}_{ijkl}\varepsilon_{ij}\varepsilon_{kl} - n_d\varepsilon_{ij}\mathrm{P}_{ij}, \quad (2)$$

where E_d is the defect formation energy. Eq. 2 identifies a mechanism for controlling the relative concentrations of the three types of oxygen vacancies. Consider a sample in the homogeneous strain state $\varepsilon_{zz} = const.$ and all other $\varepsilon_{ij} = 0$. The last term depends on the orientation of the oxygen vacancy. So, the difference in the free energy of vacancies of different orientations translates directly into a Boltzmann factor which gives the ratio of the concentrations (k_B : Boltzmann constant, T : temperature),

$$\frac{c_z}{c_{x,y}} = e^{\epsilon_{zz}(\mathrm{P}_{zz} - \mathrm{P}_{x,y})/k_B T} \quad (3)$$

A homogeneous strain state thus creates an anisotropy in the oxygen vacancy distribution. Once the vacancy distribution is no longer uniform, the uncompensated vacancies generate a non-zero strain field.

Of more practical utility, in the elastic limit, a uniaxial strain field can be created by applying a homogeneous stress σ_{zz} to the crystal. This anisotropy prevents the strain fields generated by the oxygen vacancies of different orientations from completely screening each other; only the strain field due to the uncompensated z-type oxygen vacancies remains, which can be detected by diffuse x-ray scattering.

B. Diffuse scattering from correlated oxygen vacancies

In this section, we describe the consequences of the ordering of the oxygen vacancies in $SrTiO_3$ on the scattering. The diffuse scattering for correlated defects is given by[19]

$$I(\mathbf{Q}) = \frac{|F(Q)|^2}{\Omega_c^2}\left|\sum_\mu c^\mu \mathbf{G}_n \mathrm{D}^{-1}_{ni}\mathrm{P}_{ij}\mathbf{q}_j\right|^2 \quad (4)$$

The scattering vector is $\mathbf{Q} = \mathbf{G} + \mathbf{q}$; $\mathbf{G}$ is a reciprocal lattice vector and $\mathbf{q}$ is restricted to be in the first Brillouin zone (Ω_c : the volume of the average unit cell of the crystal, c^μ : the concentration of μ-type defects, P : the elastic dipole tensor, $\mathrm{D}_{ni} \equiv \mathrm{C}_{nkmi}\mathbf{q}_k\mathbf{q}_m$, C : elastic stiffness tensor). In highly asymmetric situations such as uniaxial applied stress or biaxial substrate induced strain, only one type of oxygen vacancy (only the uncompensated portion) will contribute to the diffuse scattering due to the traceless nature of the elastic dipole tensor for oxygen vacancies in $SrTiO_3$.

First, the diffuse scattering for an isotropic concentration of $(V_O)_n$ was calculated using Eq. (4); there is no scattering in this case. Again, this is due to the traceless nature of the elastic dipole tensors of $(V_O)_n$

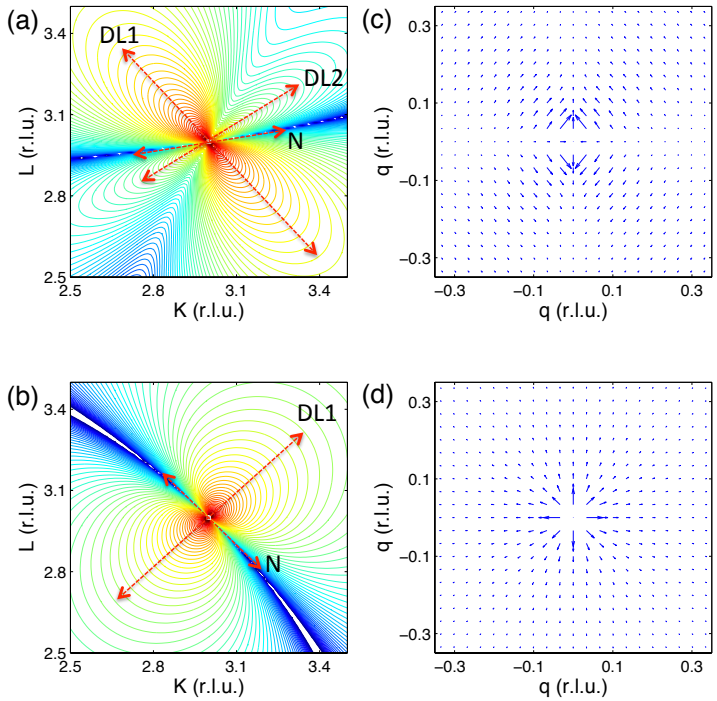

FIG. 3. (Color online) Calculated diffuse scattering from V_O in the $SrTiO_3$ crystal using (a) Freedman's elastic dipole tensor and (b) the 3×3 identity matrix as the elastic dipole tensor, and the Fourier transform of the displacement field ($\mathbf{U}(q)$) (c) and (d) calculated from (a) and (b), respectively (the calculated diffuse scatterings are shown as log-scaled contour plots in arbitrary units where red signifies maximum intensity and blue signifies minimum intensity.)

in the $SrTiO_3$ and this agrees with our previous experimental result[9]. It is worth emphasizing that the lack of a noticeable volume change is the result of the correlation between vacancies of different types. A conventional formulation for the diffuse scattering for randomly distributed defects invokes an incoherent sum of scattering intensities from the different vacancies, which is incompatible with our observations. Thus, it is likely that this can be applied the other perovskite oxide materials that show no volume change from oxygen vacancies as well.

Second, calculations were made for an anisotropic concentration of $(V_O)_n$ ($c_z/c_{x,y} = 1.4$, 40 % excess $(V_O)_z$). The calculated diffuse scattering of a $SrTiO_3$ crystal is shown in Fig. 3(a). The strong diffuse lobe (marked as DL1) lying along the (0 1 $\bar{1}$) direction has much higher intensity than the small lobe (marked as DL2). The calculated scattering also reveals that the nodal plane (marked as N) lies a little off from L = 3.0, instead of along the (0 1 $\bar{1}$) direction. In the experimental RSM (Fig. 1(c)), weaker lobe (DL2) and the nodal plane (N) are buried under the TDS and its noise due to the counting statistics of the experimental system only showing the strong lobe (DL1) on top of the TDS. Note that we arrive at the identical result when the displacement field of the sample with anisotropic concentrations is qualitatively considered due only to $(V_O)_z$, since the displacement fields from $(V_O)_{x,y}$ are canceled.

In order to compare the nature of oxygen vacancies in $SrTiO_3$ with uncorrelated isolated vacancies, we also simulated the diffuse scattering with the "conventional" isotropic dipole tensor. This was done by inserting a 3×3 identity matrix as P_{ij} in Eq. (4). The simulation result in Fig. 3(b) shows the "conventional" Huang diffuse scattering (HDS) intensity map with a nodal plane (N) along (0 1 $\bar{1}$) direction and a strong diffuse scattering (DL1) along the (0 1 1) direction. This exhibits the general features of the HDS for dilute and uncorrelated point defects. This comparison clearly demonstrates the effect of the correlation of the oxygen vacancies on the diffuse scattering symmetry.

From the simulated results of Fig. 3(a-b), one can extract the information of displacement fields induced by the point defects by using the following equations[19]

$$I(\mathbf{Q}) = \frac{|F(Q)|^2}{\Omega_c^2} \left\langle |\mathbf{G}\cdot\mathbf{U}(\mathbf{q})|^2 \right\rangle . \qquad (5)$$

Here, $\mathbf{U}(q)$ is the (continuous) Fourier transform of the displacement field. Figure 3(c) and 3(d) display $\mathbf{U}(\mathbf{q})$ corresponding to the diffuse scattering map from Fig.

3(a) and 3(b), respectively. One can see that the "conventional" dipole (Fig. 3(d)) represents a simple isotropic dilation center and that the dipole corresponding to oxygen vacancies in $SrTiO_3$ (Fig. 3(c)) displays a contraction along K and an expansion along L in this plane. Intuitively, one can expect a volume change from the "conventional" dipole tensor, but the oxygen vacancies in $SrTiO_3$ show no net dilation or contraction which results in no volume change. Thus, the anisotropy of the displacement field $\mathbf{U}(\mathbf{q})$ demonstrates the underlying correlations existing between the point defects in $SrTiO_3$.

C. q^{-3} dependence of the diffuse scattering

Here, we are interested in describing the observed q^{-3} dependence of the diffuse scattering associated with the uncompensated oxygen vacancies in $SrTiO_3$. One may expect that the correlation and screening between vacancies of different types leads to clustering. In particular, we first consider a periodic lattice of atoms with a statistical distribution of point-defect clusters. For a spherical cluster of n_{cl} isotropic point defects with displacement fields $A\mathbf{r}/r^3$ (A is constant), the diffuse scattering exhibits the classical crossover from q^{-2} (Huang scattering) at small q to q^{-4} at large q (Stokes-Wilson scattering)[20] where the crossover depends on the size of the cluster. Clearly, our data do not exhibit the q dependence associated with spherical clusters of isotropic point defects.

The q^{-3} dependence may, however, be understood in terms of non-spherical clusters of oxygen vacancies. As in the conventional case, the defect cluster size can be estimated from the position of the crossover in q. By replotting Fig. 1(a) in the log-log scale we could take the"kink" position where the diffuse profile approaches the Bragg peak as an indication of the cluster size (the inset of Fig. 1) . The inverse of this kink gives an estimate of over 90 nm for the diameter of the oxygen vacancy cluster. This distance corresponds closely to the density of dislocation pits in (0 0 1) $SrTiO_3$, which has been measured to be about 5×10^9 cm^{-2} by atomic force microscopy[21]. This intriguing coincidence suggests that the q^{-3} behavior may result from the cylindrical distribution of oxygen vacancies around oriented dislocation lines. The dominant dislocations in (0 0 1) $SrTiO_3$ are aligned along the crystal growth direction (z) and are edge-type with Burgers' vectors in $\langle 1\,0\,0\rangle$ and $\langle 1\,1\,0\rangle$ directions[22].

We calculated the energy of interaction between the uncompensated z-type oxygen vacancies and edge dislocations in the crystal. Calculations were made for Burgers' vectors along all $\langle 1\,0\,0\rangle$ and $\langle 1\,1\,0\rangle$ directions in the xy plane. Each exhibits the same behavior. For $(V_O)_z$ interacting with edge dislocations, we find that the vacancies drift towards the compressive side (blue colored region) of the dislocation in the xy plane in Fig. 4(a)[23], and that the result is independent of z.

Now assuming that the dislocations are aligned along z with $\langle 1\,0\,0\rangle$ and $\langle 1\,1\,0\rangle$ Burgers's vectors and randomly

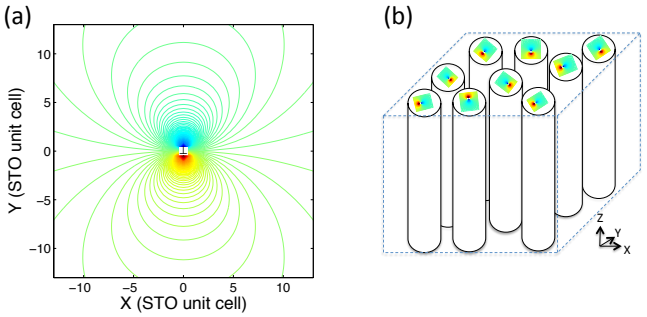

FIG. 4. (Color online) (a) Interaction energy between the edge dislocation and oxygen vacancy in $SrTiO_3$ (blue : interaction energy < 0, red : interaction energy > 0, and the contour plot is in the log-scale with the arbitrary unit) (b) schematic image for the cylindrical distribution of oxygen vacancies around the edge dislocation

located with density 5×10^9 cm^{-2}, the distribution of vacancies around dislocations averaged throughout the crystal will be cylindrically symmetric since the interaction is independent of z direction. Our model is that point vacancies are attracted to the oriented line defects, creating two-dimensional problem rather than a three-dimensional one, which is schematically presented in Fig. 4(b). The vacancies remain point objects, but the resultant displacement fields from oriented linear vacancy clusters creates the q^{-3} dependence.

To illustrate, consider a cylindrical cluster of the same point defects as above. In analogy to electrostatics, the displacement field far from the cluster has the form $\lambda A\mathbf{r}/\left(2\pi r^2\right)$ where $\lambda = \rho\pi R_{cl}^2$ is the number of defects in a unit length of the cluster, ρ is the (assumed) uniform volume density of vacancies inside the cluster and R_{cl} is the radius of the cluster. Then, we arrive at the diffuse scattering amplitude

$$A_{diff}\left(\mathbf{Q}\right) \propto \sum_j e^{i\mathbf{q}\cdot\langle\mathbf{R}_j\rangle}\left[e^{i\mathbf{G}\cdot\delta\mathbf{u}_j} - 1\right] \tag{6}$$

Note that $\left(e^{i\mathbf{Q}\cdot\delta\mathbf{u}} - 1\right)$ can be replaced by $i\mathbf{G}\cdot\delta\mathbf{u}$ for $r > R_{cl}$.

$$e^{i\mathbf{G}\cdot\delta\mathbf{u}(\mathbf{r})} \simeq \begin{cases} 0 & \text{for } r < R_{cl} \\ 1 + i\left(\mathbf{G}\cdot\mathbf{r}\right)\lambda A/2\pi r^2 & \text{for } r > R_{cl} \end{cases} \tag{7}$$

which results in a scattering intensity

$$I_{diff} \propto \left(2\pi R_{cl}^2 \frac{J_1\left(qR_{cl}\right)}{qR_{cl}} + A\lambda\frac{\mathbf{G}\cdot\mathbf{q}}{q^2}J_0\left(qR_{cl}\right)\right)^2, \tag{8}$$

exhibiting a crossover from q^{-2} for $qR_{cl} \ll 1$ to q^{-3} for $qR_{cl} \gg 1$. Hence, the scattering from cylindrical distribution of oxygen vacancies changes the q-dependence to q^{-3} but leaves the angular symmetry of the underlying $(V_O)_z$ scattering unchanged[24]. Thus, the experimental diffuse scattering profiles from the externally strained

$SrTiO_3$ crystal can be explained by the arrangement of uncompensated $(V_O)_z$ around the inherent dislocation lines. We note, however, that we cannot extract quantitative information about the oxygen vacancy concentration in $SrTiO_3$ due to the correlation of the defects.

We also considered other potential sources for the anomalous q^{-3} dependence of the diffuse scattering. Freedman *et al* calculated the dipole tensors from other energetically favorable point defects in $SrTiO_3$ such as Sr vacancies and Sr-O divacancies and we simulated the diffuse scattering from such defects. Similarly, we calculated the diffuse scattering from dislocation loops. All of these scattering results did not match the symmetry of the experimental result of Fig. 1(c) and were thus ruled out as possible sources of our observed scattering.

V. CONCLUSIONS

Our measurement and analysis of diffuse scattering of oxygen deficient $SrTiO_3$ crystals controlled by an external stress showed the following results. The diffuse scattering intensity from oxygen vacancies is not proportional to the oxygen vacancy concentration, as is generally assumed in HDS, and instead indicates correlations between vacancies of different orientations. Using the reported dipole tensor for oxygen vacancies in $SrTiO_3$ crystal, we calculated the expected diffuse scattering. The calculated symmetry of the diffuse scattering from correlated oxygen vacancies agreed well with the experimental results. We explained the q^{-3} falloff of the intensity as a result of the cylindrical distribution of oxygen vacancies around oriented dislocation lines in the crystal.

ACKNOWLEDGMENTS

We acknowledge technical assistance from J.D. Ferguson, A.F. Siliciano, and A.Y. Kazimirov; stimulating discussions with D.A. Freeman, T.A. Arias, Hui-Qiong Wang, D.G. Schlom, D.A. Muller, and P.F. Miceli; and, funding from the NSF under award DMR-0705361. This work is based upon research conducted at CHESS which is supported by the NSF and the NIH/NIGMS under NSF award DMR-0225180.

* yongsam_kim@postech.ac.kr
† joel.brock@cornell.edu

[1] A. Ohtomo, D. A. Muller, J. L. Grazul, and H. Y. Hwang, Nature **419**, 378 (2002).
[2] A. Ohtomo and H. Y. Hwang, Nature **427**, 423 (2004).
[3] M. Huijben, A. Brinkman, G. Koster, G. Rijnders, H. Hilgenkamp, and D. H. A. Blank, Adv. Mater. **21**, 1665 (2009).
[4] D. G. Schlom, L.-Q. Chen, X. Pan, A. Schmehl, and M. A. Zurbuchen, J. Am. Ceram. Soc. **91**, 2429 (2008).
[5] H. P. R. Frederikse, W. R. Thurber, and W. R. Hosler, Phys. Rev. **134**, A442 (1964).
[6] D. A. Crandles, B. Nicholas, C. Dreher, C. C. Homes, A. W. McConnell, B. P. Clayman, W. H. Gong, and J. E. Greedan, Phys. Rev. B **59**, 12842 (1999).
[7] D. A. Freedman, *Atomic Level Theory of the Growth of Crystalline Oxide Materials*, Ph.D. Thesis, Cornell University (2009).
[8] D. A. Freedman, D. Roundy, and T. A. Arias, Phys. Rev. B **80**, 064108 (2009).
[9] Y. Kim, A. S. Disa, T. E. Babakol, and J. D. Brock, Appl. Phys. Lett. **96**, 251901 (2010).
[10] L. J. van der Pauw, Philips Res. Rep. **13**, 1 (1958).
[11] L. J. van der Pauw, Philips Tech. Rev. **20**, 220 (1958).
[12] X. Fang, (2011), private Communication.
[13] D. A. Tenne, I. E. Gonenli, A. Soukiassian, D. G. Schlom, S. M. Nakhmanson, K. M. Rabe, and X. X. Xi, Phys. Rev. B **76**, 024303 (2007).
[14] W. Gong, H. Yun, Y. B. Ning, J. E. Greedan, W. R. Datars, and C. V. Stager, J. Solid State Chem. **90**, 320 (1991).
[15] H. Peisl, J. Appl. Cryst. **8**, 143 (1975).
[16] U. Schubert, H. Metzger, and J. Peisl, J. Phys. F: Met. Phys. **14**, 2457 (1984).
[17] M. Yoon, J. Z. T. B. C. Larson, T. E. Haynes, J. S. Chung, G. E. Ice, and P. Zschack, Appl. Phys. Lett. **75**, 2791 (1999).
[18] U. Beck, T. H. Metzger, J. Peisl, and J. R. Patel, Appl. Phys. Lett. **76**, 2698 (2000).
[19] H. Trinkaus, Phys. Status Solidi B **51**, 307 (1972).
[20] P. H. Dederichs, Phys. Rev. B **4**, 1041 (1971).
[21] K. Szot, W. Speier, R. Carius, U. Zastrow, and W. Beyer, Phys. Rev. Lett. **88**, 075508 (2002).
[22] J. Yoshimura, T. Sakamoto, S. Usui, and S. Kimura, J. Cryst. Growth **191**, 483 (1998).
[23] R. A. Johnson, J. Appl. Phys. **50**, 1263 (1979).
[24] C. Revenant, F. Leroy, R. Lazzari, G. Renaud, and C. R. Henry, Phys. Rev. B **69**, 035411 (2004).